Very high cycle fatigue behaviour of austenitic stainless steel and the effect of strain-induced martensite

C. Müller-Bollenhagen [a,*], M. Zimmermann [a], H.-J. Christ [a]

[a]Institut für Werkstofftechnik, Universität Siegen, 57068 Siegen, Germany

* corresponding author. Tel. +49271 740 3419

E-mail addresses: carsten.mueller-bollenhagen@uni-siegen.de (C. Müller-Bollenhagen)

martina.zimmermann@uni-siegen.de (M. Zimmermann)

hans-juergen.christ@uni-siegen.de (H.-J. Christ)

Keywords: deformation-induced martensite, austenitic stainless steel, fatigue limit, very high cycle fatigue (VHCF), plain specimens

Abstract

Metastable austenitic stainless steels are known to undergo a partial transformation of austenite into martensite as a consequence of plastic deformation. This transformation process depends on the chemical composition, the accumulative strain as well as the strain rate, the temperature and the microstructure. As most manufacturing processes of metallic components lead to plastic deformation in the material, the utilization of this transformation effect to adjust the monotonic and cyclic strength behaviour for the highly stressed areas of a component is evident. It is shown that monotonic and cyclic strength properties can be systematically changed by controlling the deformation-induced martensite content. The austenitic stainless steel studied was found to show a constant fatigue limit from 10^6 to 10^9 cycles that is primarily attributed to the strengthening effect of martensitic transformation. Load-increase tests were used to estimate an optimum martensite content in predeformed specimens to reach a maximum fatigue limit.

1. Introduction

Metastable austenitic stainless steels can undergo a deformation-induced phase transformation from austenite (fcc) into ε-martensite (hcp) and α'-martensite (bcc). Transformed α'-martensite can be used to modify monotonic [1] and cyclic [2] properties of austenitic stainless steel. This is of particular interest as austenitic stainless steels are often used for components with increasing safety requirements, like pipelines in nuclear reactors or heavy-duty automotive structures. The major aim of this study is to establish a basis for the optimization of the fatigue strength of an automotive structural part - the cross tube of a trailer coupling - by forming a specific amount of martensite during its tube-forming process. A more detailed description of this structural element and the forming process is given elsewhere [3].

The study presented aims at a comprehensive understanding of the correlation between the very high cycle fatigue (VHCF) behaviour and the martensite formation of metastable austenitic steels. Over the last decade it was shown for a number of metals that failure occurs even beyond the classical fatigue limit of $2x10^6$-10^7 cycles [4, 5]. Crack initiation gains importance at larger fatigue lives and various reports in the literature propose that localized cyclic plastic deformation and a resulting crack initiation are the dominant life controlling mechanisms [e.g. 6]. Depending on the material studied, the localized plastic deformation can lead to surface as well as subsurface crack initiation, mostly occurring at persistent slip bands or at pores or inclusions, respectively. In this context so-called dual or multistage fatigue life diagrams are being discussed. In order to distinguish between the different damage mechanisms, Mughrabi [7] suggested the classification of metals in type I materials showing surface crack initiation, typically single phase ductile metals, and type II materials with inner defects such as inclusions, pores etc. showing subsurface crack initiation.

The VHCF behaviour of AISI304 has hardly been investigated yet, especially the correlation of martensite formation and very high cycle fatigue is still basically unknown. Takahashi and Ogawa

[8] studied the fatigue behaviour of non-martensitic monotonically predeformed AISI304 specimens and observed a singular appearance of internal crack initiation (‘fish eye fracture’) in the VHCF regime. No defect in the crack-origin could be found. Hence the role of hard inclusions quite likely present in austenitic stainless steels in the crack initiation process at very high load cycles is not clear. Chai [9] observed subsurface non-defect fatigue crack origins in experiments with a non-predeformed martensite-austenite steel at cycles higher than 10^6 and concluded that the damage process in the VHCF range of two phase alloys can be determined by deformation mismatches in the two phases, as a consequence of their differing mechanical properties. For high cycle fatigue, Myeon et al. [10] detected a 60-fold enhancement of fatigue life in the HCF-regime as a result of thermally induced micro-martensite particles which prevent crack initiation. Maier et al. [2] proved that there is an optimum volume fraction of deformation-induced martensite in AISI304 of 30-40% for the low cycle fatigue regime.

The purpose of this study is to investigate the martensite formation under monotonic and cyclic loading and the influence of martensite formation through predeformation on the VHCF behaviour.

2. Materials and Methods

Three batches of stainless steel sheets (AISI304) were tested under monotonic tensile loading in the as-received condition. The composition, mechanical properties and calculated M_{d30}-temperatures [11] are shown in Table 1 and 2. The mean grain size varied between 21 and 25 µm for all batches. Isolated carbide inclusions with high Ti, Cr and Mn contents (acc. to EDS-analysis) and a size of 5-10 µm were found in SEM investigations as well as a rare occurrence of linearly arranged δ-ferrite.

The volume fraction of martensite was measured by means of the magneto-inductive device *feritscope MP30* (FISCHER). All values for martensite fraction in the following are the values measured by feritsope; where applicable the value were corrected by functions taking into account

variation in measured values for geometrical or loading reasons (Villari-Effect). The aspect that results measured via feritscope might underestimate the true martensite fraction [12] will be further investigated and should be taken into account when comparing results from different studies.

For the tensile tests at room temperature an electromechanical testing machine was applied. For the tensile tests below room temperature a hydraulic testing machine equipped with a liquid-nitrogen-cooled chamber was used. All tensile tests were performed with in-situ measurements of temperature and martensite content (feritscope).

For the fatigue experiments a resonance pulsating high-frequency test system operating at 90 Hz and an ultrasonic testing machine operating at a test frequency of around 20 kHz were used. The vibrating parts of the ultrasonic testing system are designed in a way that under resonance conditions a standing wave develops along the major load axis with a maximum stress/strain amplitude in the center region of the specimen (Fig. 1). At this center region strain gauges are used to measure the strain amplitude in order to calibrate the initial load/displacement control signal. A cyclic stress-strain curve, registered during the resonance pulsating experiments, was used to determine the corresponding stress amplitude for any such measured strain amplitude. The fatigue tests were conducted under axial tension-compression loading with a stress ratio of R = -1 in ambient air, applying intermitting pulse and pause sequences for the ultrasonic testing (typical pulse/pause length: 90 ms/2000 ms).

Temperature was measured at three points of the specimen with a thermal infrared camera (FLIR A20-M) and K-type thermocouples. As has been proposed by Smaga et al. [13] the change of temperature ΔT was used to describe the cyclic deformation behaviour. The location of the measured temperatures and the specimen geometry used are illustrated in Fig. 2. ΔT was calculated using the equation

$$\Delta T = T_1 - 0.5 \cdot (T_2 + T_3). \quad (1)$$

According to refs. [14, 15] load-increase tests accompanied by high resolution temperature measurement can be used to estimate the fatigue limit of metals. This method was used at the resonance pulsating test system for a preliminary comparison of the fatigue limits of specimens with different martensite fractions.

Fatigue experiments executed by means of the resonant vibrating system were stopped after 10^8 cycles, ultrasonic fatigue tests after 10^9 cycles. Corresponding specimens without appreciable cracks were denoted as run-outs. Specimens were electro-chemically polished, except the predeformed specimens that were mechanically polished. Because of its low thermal conductivity, good damping properties and relatively high ductility, the materials used showed a strong development of heat and the testing in both systems required an active cooling with compressed air.

3. Results and discussion

3.1 Martensite formation and damage behaviour under monotonic loading.

Tensile tests were performed to quantify the major factors affecting deformation-induced martensite formation. Different start temperatures during tensile testing can be used to adjust the quasi-static mechanical properties, Fig. 3. With a decrease of the specimens initial temperature from 23°C to -20°C the stress-strain curve changes from a parabolic to a more sigmoidal shape caused by an increasing volume of α'-martensite. This leads to an increase in tensile strength of about 30 % and a decrease in elongation at fracture.

Furthermore, it can be stated that the martensite formation strongly depends on the batch-specific chemical composition. Figure 4 correlates reasonably with the M_{d30} temperatures in Table 2, with the batch HR having the strongest affinity to martensite formation and batch TK the weakest. However, M_{d30} can only give a coarse account of the austenite stability, as the significant

differences in martensite formation of batches HR and WS in Fig. 4 was not expected. Moreover, the strain rate strongly influenced the martensite formation during tensile testing.

Colour-etched micrographs of the tensile specimens show a strong formation of ε-martensite during the initial state of deformation. Up to a deformation of 10% mainly ε-martensite and only isolated areas of α'-martensite formation can be found (Fig. 5). The small dark needles in Fig. 5a are assumed to be ε-martensite. This is confirmed by the low fraction of magnetic phase in this state (0.6 vol-%). The needles are mostly tilted at a degree of 45° to the loading direction. Where they cross each other α'-martensite nucleates. Figure 5b) illustrates the preferred transformation of α'-martensite in horizontal lines, which are most likely a consequence of micro-segregations. For all batches similar lines of α'-martensite can be observed as well as an accumulation of α'-martensite in the middle of the cross-section of the sheet.

The tensile test results were used to determine the consistency of acknowledged material models from literature to predict the martensite formation resulting from a monotonic uniaxial deformation. Three models proposed by Springub et al. [16], Hänsel [17] and Picozzi et al. [18] were surveyed. Because of the mentioned batch variations it is necessary to fit specific constants for each model with batch-specific tensile test data. All models show a satisfactory agreement between experimental and calculated data for tensile tests at room temperature for the batch HR. Details concerning this study are given in [3]. Further investigations with varying parameters (strain rate, ambient temperature etc.) will lead to a precise evaluation of the ability of these models to predict martensite formation in sheet forming processes.

3.2 Damage behaviour under cyclic loading.

Fatigue tests were conducted in order to characterize the VHCF behaviour of AISI304 in fully austenitic and partially martensitic state. Only specimens made of batch HR were fatigued, because this batch showed the strongest affinity to martensite formation. A distinct cyclic softening followed

by a cyclic hardening could be observed during all fatigue experiments, even though stress amplitudes were considerably below 0.2% yield stress $R_{p0.2}$ and even below the fatigue limit at 10^8 cycles. Fig. 6 shows an increase in ΔT up to about $7x10^4$ cycles followed by a decrease in ΔT up to approx. 3×10^6 cycles for a run-out specimen tested at σ_a = 240 MPa. Earlier studies on the correlation of plastic strain and ΔT performed by various authors [14, 19-22] have proven that ΔT can be used to describe the cyclic deformation behaviour in load-controlled tests for many materials including the metastable austenitic steel used in this study. Both signals (ΔT as well as plastic strain) rise when cyclic softening emerges and decrease for cyclic strengthening. Therefore, in Fig. 6 the increasing ΔT documents cyclic softening to take place up to $7x10^4$, followed by cyclic hardening (decreasing ΔT). The same trend exists for the course of the test frequency, which is the resonance frequency of the specimen-machine system (Fig. 6). Both parameters, temperature and test frequency, can be used to monitor the transient behaviour of the material during cyclic deformation. Frequency changes attributed to machine parameters or other external influence factors can be excluded, as testing conditions were kept constant. The temperature and frequency changes during the initial 10^6 cycles illustrate that the material studied does experience global plastic deformation before reaching a saturation stage. For this reason, the damage mechanism in the VHCF region cannot be attributed to the phenomenon of inhomogeneously distributed local plastic deformation. The global plastic deformation, as is shown in Fig. 6, has to be considered, too.

Load-increase tests were performed to estimate the fatigue limit of the material studied on the basis of ΔT. In Fig. 7 the changes in temperature ΔT for two fully austenitic, non-predeformed specimens during a stepwise load-increase test are plotted versus the number of cycles. During the test sequence the stress amplitude was increased by 10 MPa each 10^4 cycles. In order to avoid any interfering influences because of slightly different cooling conditions no active cooling was applied during the load-increase tests. ΔT was measured by means of the infrared camera. In Fig. 7 it can be

seen that the change of temperature ΔT rises with every step but converges to a horizontal asymptote within every step up to 240 MPa, where it starts to rise significantly and continuously. The correlation between ΔT and the plastic strain amplitude has already been discussed before. In this context a prediction of the fatigue limit based on load-increase tests accompanied by the measurement of a change in ΔT has also been widely analysed [14,15,19,22]. Among other authors Cugy and Gaultier [23] showed for low carbon steel that an increasing development of heat in load-increase tests is related to an increasing appearance of slip bands on the specimen surface. At the same time they point out that there are limitations in the prediction of the fatigue limit in load-increase tests [23]. They demonstrate that different materials with the same fatigue limit can show a very different development of heat. Nonetheless, in the presented study a thermographic prediction of the fatigue limit seems to be an appropriate approach, because specimens of the same material are compared in different conditions. Taking the aforementioned studies into account, a first assessment of the fatigue limit on the basis of load-increase tests for the same material in different conditions is justified. In this study, the fatigue limit is assumed as the first load amplitude level where the ΔT value does not converge to a horizontal asymptote. In Fig. 7, 240 MPa is therefore taken as a first assessment of the fatigue limit for the fully austenitic condition.

This fatigue limit was subsequently confirmed by means of constant amplitude tests. The results are shown in Fig. 8. These tests were executed on the resonance pulsating system up to 10^8 cycles. The fatigue limit resulting from the constant amplitude tests is 250 MPa. No failure occurred between 10^6 and 10^8 cycles. All failed specimens were loaded at stress amplitudes above 250 MPa. Metallographic analysis of the fracture surfaces proved that no subsurface crack initiation had occurred.

As the investigated material shows considerable cyclic hardening and softening, the ultrasonic system could not be used to cycle specimens from the beginning. The closed-loop control system of

the ultrasonic system only guarantees a constant load amplitude, when the global plastic deformation is small. For this reason, specimens where cycled up to 10^6 by means of the resonance pulsating system, thus reaching the cyclic saturation stage (Fig. 6). Subsequently specimens were fatigued by ultrasonic testing up to 10^9 cycles. The load amplitude for the ultrasonic system was calibrated based on a cyclic stress-strain curve recorded for several specimens at 10^6 cycles with the resonance pulsating system by the use of strain gauges in combination with the respective load cell. The results of two ultrasonic fatigued specimens are shown on the right-hand side of Fig. 8. Both tests led to run-outs and, hence, support the fatigue limit at 250 MPa. The formation of α'-martensite needles in isolated grains (Fig. 9a) and slip bands in most grains (Fig. 9b) at the surface of all run-out specimens are an indication of local plastic deformation. No decrease in the fatigue limit in the VHCF regime and no failure of specimen above 10^6 cycles occurred.

Load-increase tests were used to study the dependence of the fatigue limit of austenitic specimens on the deformation-induced martensite content. The different martensite contents were adjusted by means of a 15% elongation by a tensile load at different temperatures below room temperature. Subsequently these specimens were mechanically polished and fatigued by load-increase tests with a step length of 10^4 cycles and a step height of 5 MPa. Thermocouples were spot welded on the gauge length of the specimens, leading to small notches at the surface. In Fig. 10, the results for four specimens containing volume fractions from 1% up to 34% martensite are shown. All tests were executed until failure of the specimen. Comparing the samples with 1% and 19% martensite volume fraction, a strong increase in the stress amplitude, which leads to a significant temperature change indicating specimen failure, can be observed (from 345 MPa to 380 MPa). However, with increasing martensite content (26% and 32%) the stress amplitude resulting in specimen failure and abrupt rise in ΔT decreases again (Fig. 10). Hence, an optimal martensite content with regard to the fatigue limit can be assumed to exist at a volume fraction below 26% as a first approach for specimens with a small notch and under the given testing conditions. Constant amplitude tests with

varying martensite contents will be executed to verify the assessed optimal martensite content during the continuation of the present work.

The main effects on the fatigue limit that appear to be most relevant for the conducted load-controlled tests can be divided into two categories: the influence of martensite formation on the one hand and the influence of the surface conditions of the specimens (notches), as well as the influence of test parameters (frequency and temperature) on the other hand. These influence factors and their interactions are given schematically in Fig. 11 and will now be analyzed in detail.

Two effects of martensite formation on the fatigue limit and the VHCF behaviour were observed: the effect of martensite from predeformation and the effect of martensite transformed during cyclic loading. Martensite that is induced by monotonic predeformation significantly increases the fatigue limit until a specific volume fraction is reached. Using load-increase tests, this optimum volume fraction were determined to be about 19 vol-% of martensite (Fig. 10). The increase in the fatigue limit with increasing martensite content originates from the higher strength of the martensite phase and the therefore lower plastic strain amplitude for a given load.

Furthermore, martensite that is formed during cyclic loading influences the fatigue limit, although the content of martensite that was found in specimens after cyclic loading is small (less then 3% for all specimens in Fig. 8). Martensite is formed locally on the active slip systems (Fig. 5a and 8a) that are often tilted 45° to the load direction because of the prevailing maximum Schmid factor. Martensite impedes dislocation motion and thus leads to a strengthening effect. This effect can be seen in Fig. 6 as cyclic hardening (decrease of ΔT) after about 10^5 cycles. Nebel [19] showed that the beginning of cyclic hardening in metastable austenites clearly correlates with an increase of martensite content. Since martensite is only transformed in isolated grains, the martensite fractions that cause the cyclic hardening are astonishingly small. The aforementioned strengthening effect of martensite formation is assumed to be the reason for the absence of failure of

specimens above 10^6 cycles. Because of the strengthening effect of martensite formation during the first 10^6 cycles, the total strain amplitude introduced by means of the load controlled tests contains only very small plastic strain (Fig. 6) for the remaining lifetime. This assumption is underlined by ΔT almost being zero in this range. This very low plastic strain amplitude yields a constant fatigue limit up to at least 10^9 cycles. SEM investigation of the surface of a specimen after 10^6 and 10^9 cycles proved that there is no increase in locally formed slip bands and martensite needles after 10^6 cycles anymore. The formation of martensite is consequently assumed to be a major reason for the specific VHCF behaviour of the analyzed material, what means

1. no decreased fatigue limit at very high number of cycles and

2. no failure of specimens above 10^6 cycles.

Another fatigue limit enhancing effect of α'-martensite formation can be attributed to compressive residual stresses after phase transformation at the plastic zone of the crack tip, caused by the higher specific volume of the α'-martensite phase [2]. The resulting lower stress intensity factors can decelerate crack-propagation. However, since in the high and very high cycle regime crack initiation is the dominant life controlling mechanism [6], this effect seems to be of minor importance here.

Apart from the influence of martensite, test parameters like frequency and temperature as well as the surface condition of specimens (notches) were found to influence the fatigue limit. To some extent they have a direct influence on the fatigue limit, but also interact with the martensite formation (Fig. 11).

Firstly the effect of the surface condition on the fatigue limit appears to vary with the martensite content induced by predeformation. An increasing notch sensitivity due to the high strength of martensite is assumed to be the reason for the decrease of the fatigue limit in load-increase tests

above 19 vol-% of martensite. Topic et al. [24] also observed an increasing notch sensitivity with increasing predeformation and martensite content at AISI304 wires. By examining the fracture surface of the 19, 26 and 34 vol.-% specimens, the notches caused by the thermocouples could be identified as site of crack initiation. First load-increase tests with unnotched specimens do not show the same correlation between optimum martensite volume fraction and fatigue limit. However, considering mechanically loaded sheet metal structures in the automotive industry, the notched condition (e.g. due to small surface defects) will be the more relevant one.

Under highfrequency testing the influence of frequency and temperature have to be coherently discussed. The test frequency directly influences the temperature of the specimen because there is less time for heat dissipation. Furthermore, higher test frequencies lead to higher strain rates. Cyclic tests conducted by Nikitin and Besel [25] at frequencies between 0.05 Hz and 10 Hz, as well as the tensile tests in this study showed an increase of the yield point with increasing strain rate. As a consequence, it must be concluded for fatigue tests at a given constant load amplitude that test frequencies of 20 kHz and 90 Hz provoke different flow stresses and therefore different plastic strain amplitudes. The lower plastic strain amplitude should lead to a higher fatigue limit, if the plastic strain is supposed to be the life-controlling damage parameter.

It was shown in refs. [19, 25] that an increasing temperature of a specimen, caused by external heating or frequency increase, produces an increased plastic strain amplitude because of the suppression of cyclic strengthening through martensitic transformation. Nikitin and Besel [25] proved that the temperature effect overcompensates the strain rate effect if specimens are not cooled. The specimens in the present study were cooled by compressed air, leading to the suppression of strong heating, but not precisely to isothermal conditions. The effect of an increased plastic strain amplitude due to the combined influence of frequency and temperature was not confirmed by the test results obtained, as an earlier failure of the ultrasonic test specimens was not

observed. Unfortunately, a total elimination of the temperature effect at 90 Hz or even 20 kHz in order to separate temperature and frequency effect is not feasible with reasonable effort for sheet specimens. Since the plastic strain amplitude after 10^6 cycles is very small for VHCF tests, the question of the influence of the test frequency and temperature on the *local* plastic deformation might be the more relevant one and will be further investigated by the authors.

4. Conclusions

The influence of deformation-induced martensite formation on the monotonic and cyclic strength of a metastable austenitic steel was studied and led to the following results:

- The susceptibility of the austenitic phase to deformation-induced martensite formation is strongly affected by temperature, strain rate and slight variations in the chemical composition.
- Constitutive material models for predicting the martensite volume fraction show a satisfactory accordance between experimentally obtained and calculated data for tensile tests at room temperature.
- The fatigue limit was estimated on the basis of load-increase tests with a difference of 10 MPa in comparison with the fatigue limit derived from constant-amplitude tests.
- The cyclic deformation was dominated by initial cyclic softening and a subsequent cyclic hardening up to a number of cycles of 10^6 merging into a saturation stage for the remaining fatigue test.
- No specimens in the undeformed condition failed in the very high cycle fatigue range, even though slip markings were observed in most grains and evidence of martensite formation was found in some grains on the samples surface.

- The fatigue limit determined by means of load-increase tests of predeformed specimens showed an optimum for a martensite volume fraction which was below 26%.

- Martensite, whether formed through cyclic or monotonic plastic deformation, strongly influences the fatigue limit and causes a strong sensitivity of the fatigue limit to the test conditions.

Acknowledgement

The authors gratefully acknowledge financial support of this study by Deutsche Forschungsgemeinschaft (DFG).

References

[1] Hecker SS, Stout MG, Staudhammer KP, Smith JL. Effects of strain state and strain rate on deformation-induced transformation in 304 stainless steel: part I. Magnetic measurements and mechanical behaviour, Metall Trans A 1982;13A:619-626.

[2] Maier HJ, Donth B, Bayerlein M, Mughrabi H, Maier B, Kesten M. Optimierte Festigkeitssteigerung eines metastabilen austenitischen Stahles durch verformungsinduzierte Martensitumwandlung bei tiefen Temperaturen. Z Metallkd 1993;84(12):820-26.

[3] Müller-Bollenhagen C, Zimmermann M, Christ H-J, Schröder X, Engel B, Große-Wöhrmann A, Suttmeier F-T. Modelling and closed-loop control of complex tube forming based on an optimized application of martensite formation in austenitic stainless steels. Steel Res Int 2008;79(10):745-752.

[4] Murakami Y, Nomoto T, Ueda T. Factors influencing the mechanism of superlong fatigue failure in steels. Fatigue & Fract Engng Mater Struct 1999;22(7):581-590.

[5] Papakyriacou M, Mayer H, Pypen C, Plenk Jr H, Stanzl-Tschegg S. Influence of loading frequency on high cycle fatigue properties of b.c.c. and h.c.p. metals. Mater Sci Eng A 2001;308(1-2):143-152.

[6] Lukáŝ P, Kunz L. Specific features of high-cycle and ultra-high-cycle fatigue. Fatigue & Fract. Engng Mater Struct 2002;25(8-9):747-753.

[7] Mughrabi H. On 'multi-stage' fatigue life diagrams and the relevant life-controlling mechanisms in ultrahigh-cycle fatigue. Fatigue & Fract Engng Mater Struct 2002;25(8-9):755-764.

[8] Takahashi K, Ogawa T. Evaluation if giga-cycle fatigue properties of austenitic stainless steels using ultrasonic fatigue test. J Solid Mech Mat Eng 2008;2(3):366-373.

[9] Chai G. The formation of subsurface non-defect fatigue crack origins. Int J Fatigue 2006;28(11):1533–1539.

[10] Myeon TH, Yamabayashi Y. Shimojo M, Higo Y. A new life extension method for high cycle fatigue using micro martensitic transformation in austenitic stainless steel. Int J Fatigue 1997;19(93):69-73.

[11] Nohara K, Ono Y, Ohashi N: Composition and grain size dependencies of strain-induced martensitic transformation in metastable austenitic stainless steels. J Iron Steel Inst Jpn 1977; 63(5):212-222.

[12] Talonen J, Aspergren P, Hänninen H. Comparison of different methods for measuring strain induced α'-martensite content in austenitic steels. Mat Sci Tech 2004;20(12):1506-1512.

[13] Smaga M, Walther F, Eifler D. Investigation and modelling of the plasticity-induced martensite formation in metastable austenites. Int J Mat Res 2006;97(12):1648-55.

[14] Wagner V, Ebel-Wolf B, Walther F, Eifler D. Very high cycle fatigue of railway wheel steels. Proc. of the 4. Int. Conf. on Very High Cycle Fatigue, Allison JE, Jones JW, Larsen JM, Ritchie RO, editors. TMS Publications, 2007, pp. 137-142.

[15] Dengel D, Harig H. Estimation of the fatigue limit by progressively increasing load tests. Fatigue Fract Eng M 1980;3(2):113-128.

[16] Springub B, Behrens BA, Doege E. Transformation induced martensite evolution in metal forming processes of stainless steels. Steel Res Int 2004;75(7):475-482.

[17] Hänsel, A. Nichtisothermes Werkstoffmodell für die FE-Simulation von Blechumformprozessen mit metastabilen austenitischen CrNi-Stählen. Dissertation, ETH Zürich, Switzerland, 1998.

[18] Piccozi V, Sanchez R, Bolt P. Improvement in constitutive equations for forming of austenitic stainless steel sheets. Final Report on the project EUR 21143, European Commission, Luxemburg, 2004, ISBN 92-894-8097-1.

[19] Nebel T. Verformungsverhalten und Mikrostruktur zyklisch beanspruchter metastabiler austenitischer Stähle. Dissertation, Universität Kaiserslautern, Germany, 2002.

[20] Nebel T, Martin U, Eifler D. Wechselverformungsverhalten metastabiler austenitischer Stähle. Härterei Tech. Mit. 2001;56(5):314-320

[21] Starke P, Walther F, Eifler D. Phybal - A new method for lifetime prediction based on strain, temperature and electrical measurements. Int J Fatigue 2006;28(9):1028-1036

[22] Cura F, Curti G, Sesana R. A new iteration method for the thermographic determination of fatigue limit in steels. Int J Fatigue 2005;27(4):453-459

[23] Cugy P, Galtier A. Microplasticity and temperature increase in low carbon steel. Proc. of the 8th int. fatigue congress, vol. 1, Blom AF, editor. EMAS, 2007, pp. 549-556.

[24] Topic M, Tait RB, Allen C. The fatigue behaviour of metastable (AISI-304) austenitic stainless steel wires. Int J Fatigue 2007;29(4):656–665.

[25] Nikitin I, Besel M. Effect of low-frequency on fatigue behaviour of austenitic steel AISI304 at room temperature and 25 °C. Int J Fatigue 2008;30(10-11):2044–2049.

List of captions

Fig. 1. Stress distribution and specimen design for the ultrasonic testing (thickness: 2mm).

Fig. 2. Specimen design and points of temperature measurement for the resonance pulsating test system (thickness: 2mm).

Fig. 3. Martensite formation in tensile tests with different start temperatures (batch HR).

Fig. 4. Influence of batch variation on martensite formation.

Fig. 5. Tensile specimens (batch WS) after a) 10% elongation, 0.6 vol-% martensite and b) 40% elongation, 14 vol-% martensite.

Fig. 6. ΔT (measured by infrared camera) and test frequency during cyclic deformation of a run-out specimen (σ_a=240MPa).

Fig. 7. Load-increase tests with fully austenitic specimen.

Fig. 8. S-N curve of electro-chemically polished specimens fatigued by resonance pulsation and ultrasonic testing (arrows indicate run-out. specimens).

Fig. 9. Martensite needles after 10^9 cycles (σ_a = 245 MPa) in some grains (a) and slip bands in most grains (b).

Fig. 10. Load-increase tests with specimens of different martensite content. The predeformed specimens were mechanically polished and thermocouples were spot welded.

Fig. 11. Effects on the fatigue limit and their interaction.

Tables

Table 1. Chemical composition [mass-%] of the alloys studied.

	C	*Cu*	*Cr*	*Mo*	*Ni*	*Mn*	*N*
HR	0.024	0.14	18.3	0.04	8.11	1.43	0.067
WS	0.04	0.23	18.2	0.20	8.05	1.19	0.049
TK	0.03	0.4	18.2	0.22	8.15	1.29	0.068

Table 2. Tensile test data and M_{d30}-temperatures.

	Young's-Modulus [GPa]	*$R_{p0,2}$ [MPa]*	*$R_{p0,1}$ [MPa]*	*R_m [MPa]*	*M_{d30} [°C]*
HR	189.7	284	266	649	2.8
WS	190.1	286	259	687	2.5
TK	194.4	300	266	641	-10.4

Figures

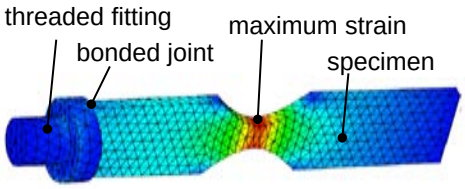

Fig. 1. Stress distribution and specimen design for the ultrasonic testing (thickness: 2mm).

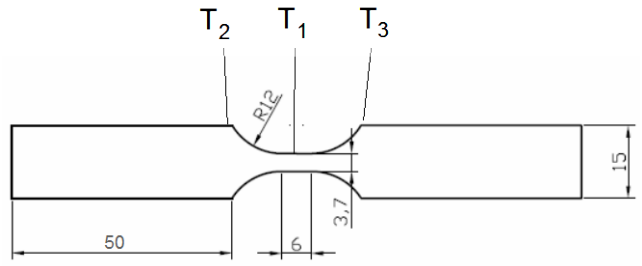

Fig. 2. Specimen design and points of temperature measurement for the resonance pulsating test system (thickness: 2mm).

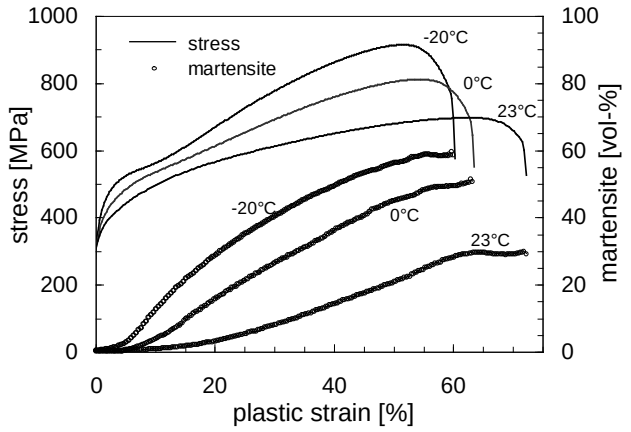

Fig. 3. Martensite formation in tensile tests with different start temperatures (batch HR).

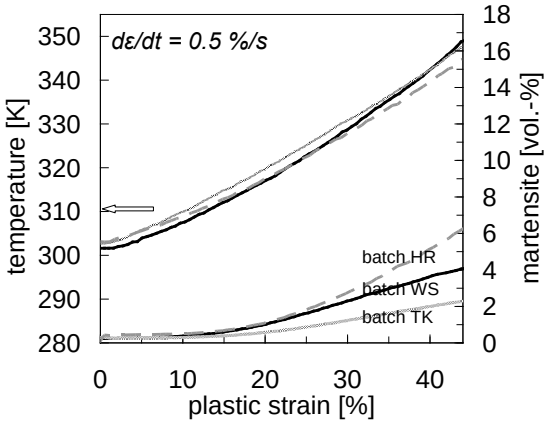

Fig. 4. Influence of batch variation on martensite formation.

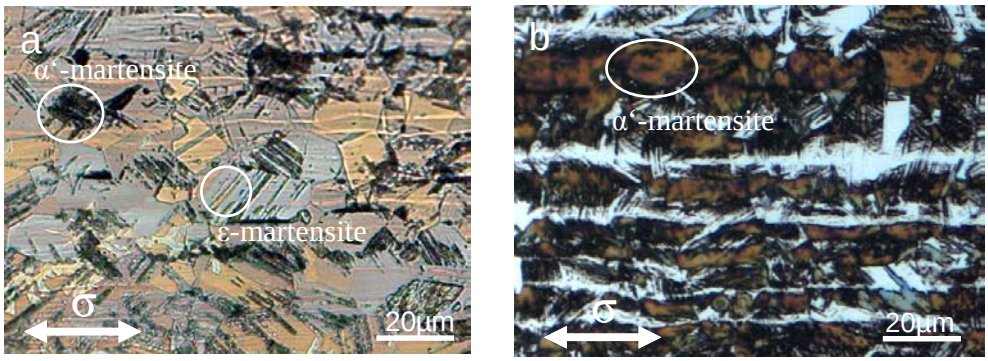

Fig. 5. Tensile specimens (batch WS) after a) 10% elongation, 0.6 vol-% martensite and b) 40% elongation, 14 vol-% martensite.

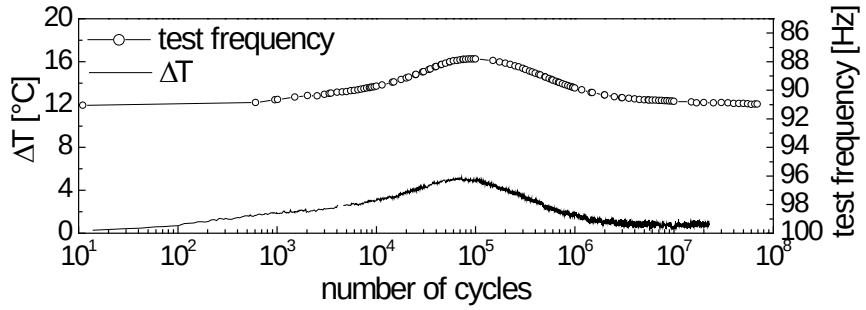

Fig. 6. ΔT (measured by infrared camera) and test frequency during cyclic deformation of a run-out specimen (σ_a=240MPa).

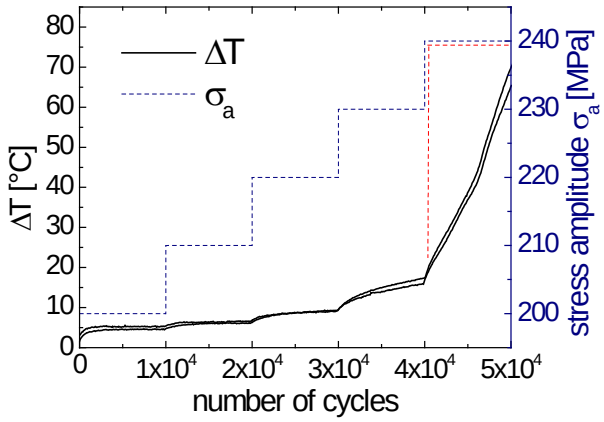

Fig. 7. Load-increase tests with fully austenitic specimen.

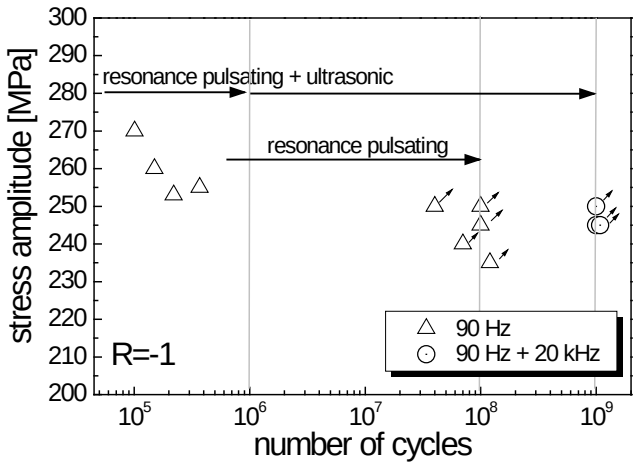

Fig. 8. S-N curve of electro-chemically polished specimens fatigued by resonance pulsation and ultrasonic testing (arrows indicate run-out specimens).

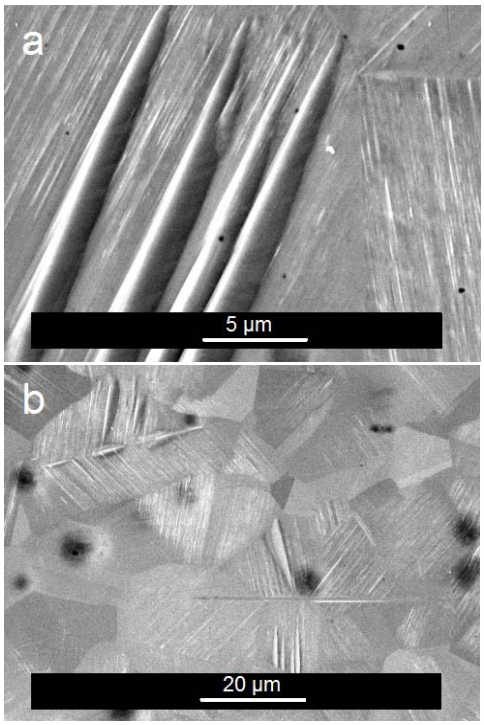

Fig. 9. Martensite needles after 10^9 cycles (σ_a = 245 MPa) in some grains (a) and slip bands in most grains (b).

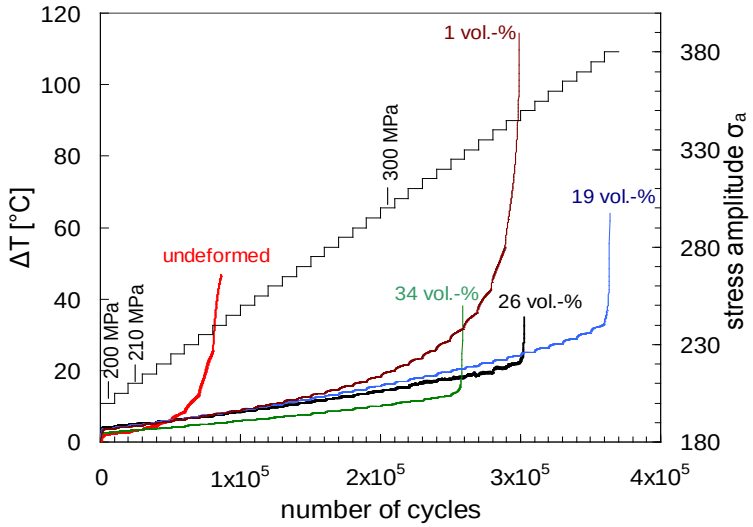

Fig. 10. Load-increase tests with specimens of different martensite content. The predeformed specimens were mechanically polished and thermocouples were spot welded.

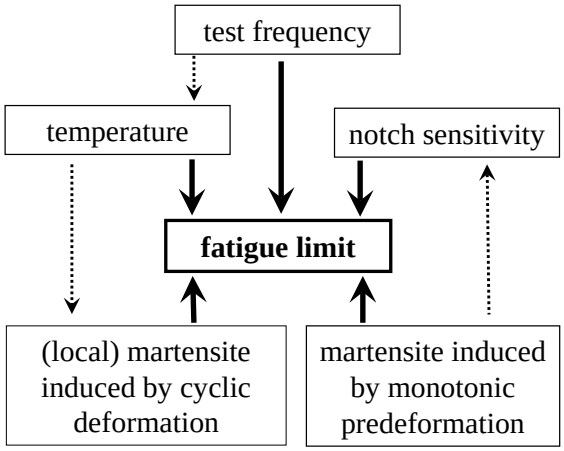

Fig. 11. Effects on the fatigue limit and their interaction.